Liquid Crystals
Publication details, including instructions for authors and subscription information:
http://www.informaworld.com/smpp/title~content=t713926090

Observation of a hexagonal blue phase in systems with negative dielectric anisotropy

G. Heppke[a]; B. Jérôme[b]; H-S. Kitzerow[a]; P. Pieranski[b]
[a] Sekretariat ER 11, Iwan-N.-Stranski-Institut, Technische Universität Berlin, Berlin, F. R. Germany [b] Faculté des Sciences, Laboratoire de Physique des Solides, Université de Paris-Sud, Orsay Cédex, France

To cite this Article Heppke, G. , Jérôme, B. , Kitzerow, H-S. and Pieranski, P.(1989) 'Observation of a hexagonal blue phase in systems with negative dielectric anisotropy', Liquid Crystals, 5: 3, 813 — 828
To link to this Article: DOI: 10.1080/02678298908026387
URL: http://dx.doi.org/10.1080/02678298908026387

LIQUID CRYSTALS, 1989, VOL. 5, NO. 3, 813–828

Observation of a hexagonal blue phase in systems with negative dielectric anisotropy

by G. HEPPKE†, B. JÉRÔME‡, H.-S. KITZEROW† and P. PIERANSKI‡

† Iwan-N.-Stranski-Institut, Sekretariat ER 11, Technische Universität Berlin, Straße des 17. Juni 135, D-1000 Berlin 12, F.R. Germany

‡ Laboratoire de Physique des Solides, Bâtiment 510, Université de Paris-Sud, Faculté des Sciences, F-91405 Orsay Cédex, France

The occurrence of a three dimensional hexagonal blue phase BPH (possible space groups $P6_222$ and $P6_422$) in materials with negative dielectric anisotropy $\varepsilon_a = \varepsilon_\parallel - \varepsilon_\perp$ has been detected by the investigation of Kossel diagrams. This is the first observation of a field-induced transition between different blue phase modifications for systems with $\varepsilon_a < 0$. BP I as well as BP II can be transformed to BPH at a sufficiently high field strength E_{BP-BPH}. For neither transitions has any discontinuity of the wavelength of selective reflection in the field direction been observed. Investigations for field strengths $E < E_{BP-BPH}$ show continuous deformation and reorientation of BP I and BP II. Decreasing (increasing) lattice constants in the field direction are found for BP I oriented with a two-fold (four-fold) axis parallel to **E** and for BP II oriented with either a four-fold or two-fold axis parallel to **E**. The preferred orientation in the field is the same as that found for $\varepsilon_a > 0$ (four-fold axis parallel to the field direction).

1. Introduction

In liquid crystals with high chirality (cholesteric pitch $< 1\,\mu$m) up to three modifications of the blue phases, referred to as BP I, BP II and BP III, can occur in the temperature region close to the clearing point [1]. These phases are characterized by a double twisted structure of the mean molecular orientation. Whereas BP III exhibits an amorphous structure, for BP I and BP II disclinations form a cubic lattice which can be described by body centred ($I4_132/O^8$) and simple cubic ($P4_232/O^2$) space groups, respectively. Because of the size of the lattice constants (of the order 10^{-7}–10^{-6} m), Bragg scattering is observed in the visible wavelength range.

Under the influence of an electric field the unit cells of the cubic structures are continuously deformed, which can be observed experimentally by a shift of the wavelength λ_{hkl} of the Bragg peaks [2]. Depending on the orientation of the unit cell with respect to the field direction, tetragonal, orthorhombic and trigonal space groups have to be considered in order to describe the continuously deformed structures [3]. For materials with positive dielectric anisotropy ($\varepsilon_a = \varepsilon_\parallel - \varepsilon_\perp > 0$) discontinuous changes of the lattice constants can also be observed [2] as a function of the field strength. It has been shown that these changes are due to the appearance of additional phases with tetragonal structure ($I4_122/D_4^{10}$, 'BPX') [4], three dimensional hexagonal ($P6_222/D_6^4$, 'BPH^{3D}') [5] and two dimensional hexagonal structures ('BPH^{2D}') [6, 7]. The stability of hexagonal blue phases in an electric field has also been considered theoretically [8, 9].

In this paper results of investigations on materials with negative dielectric anisotropy in the electric field are presented. Since, for these materials the director is forced by an electric field to align perpendicular to the field direction, they show different behaviour

0267-8292/89 $3.00

from that of systems with $\varepsilon_a > 0$. Earlier studies [10, 11] on one of these systems with negative dielectric anisotropy have shown that for BP I ([110] ∥ **E**) and BP II ([100] ∥ **E**) the lattice constant in the field direction can decrease with increasing field strength. (For materials with $\varepsilon_a > 0$ the inverse effect is observed.) Here, studies using the Kossel diagram technique are presented. The method allows the investigation of periodicities in the blue phase structure for which the reciprocal lattice vectors are not parallel to the viewing direction. With this additional information the space groups, or at least the crystal classes of the deformed blue phase structures, can be determined.

2. Origin and interpretation of Kossel diagrams

Kossel diagrams occur due to Bragg scattering if monocrystals are irradiated by convergent beams of monochromatic radiation or if a source of divergent radiation is inside the crystal [12]. For blue phases the lattice constants of the periodic structure are of the same order of magnitude as the wavelength of visible light. Thus, light in the visible wavelength range is subject to Bragg scattering and Kossel diagrams can be observed in the focal plane of the objective when studying blue phase monocrystals microscopically [4].

In this case the Bragg condition is

$$\lambda = \tilde{\lambda}\bar{n}(\lambda) = \lambda_{hkl}\frac{\bar{n}(\lambda)}{\bar{n}(\lambda_{hkl})}\cos\theta = 2\bar{n}(\lambda)\,d_{hkl}\cos\theta, \tag{1}$$

where d_{hkl} is the interplanar spacing of planes described by the Miller indices (h, k, l), θ is the scattering angle, $\bar{n}$ a mean refractive index, $\tilde{\lambda}$ is the wavelength of the scattered light propagating in the sample and λ the corresponding wavelength outside the sample. In reciprocal space equation (1) can be written, as usual, in terms of wave-vectors **k** and **k′** of the incident and the scattered light and a reciprocal lattice vector **q** corresponding to the set of planes (h, k, l)

$$\mathbf{k} - \mathbf{k}' = \mathbf{q} = h\mathbf{a}^* + k\mathbf{b}^* + l\mathbf{c}^*, \tag{1a}$$

with

$$|\mathbf{k}| = |\mathbf{k}'| = \frac{2\pi}{\tilde{\lambda}} = \frac{2\pi\bar{n}}{\lambda} \quad \text{and} \quad |\mathbf{q}| = \frac{2\pi}{d_{hkl}}.$$

If the sample is illuminated with convergent monochromatic light, the angle θ can vary from 0 to $\pi/2$ and reflection can be observed for sets of planes (h, k, l) fulfilling the condition

$$d_{hkl} > \lambda/2\bar{n}(\lambda) \tag{2}$$

or in reciprocal space

$$|\mathbf{q}| < 2\,|\mathbf{k}|. \tag{2a}$$

The scattered rays form a cone around the reciprocal lattice vector **q** which is normal to the set of planes (h, k, l). The aperture angle 2θ of the cone is given by $\cos\theta = |\mathbf{q}|/(2|\mathbf{k}|)$. The resulting Kossel diagram can be easily constructed in reciprocal space by means of a sphere with radius $R = 2|\mathbf{k}|$ (twice as large as the Ewald sphere) which is centred at the origin of the reciprocal lattice (see figure 1). Each reciprocal lattice point (h, k, l) inside the sphere represents a set of planes for which equations (2 and 2 *a*) are valid. The respective Kossel line is given by the intersection of the sphere with a plane

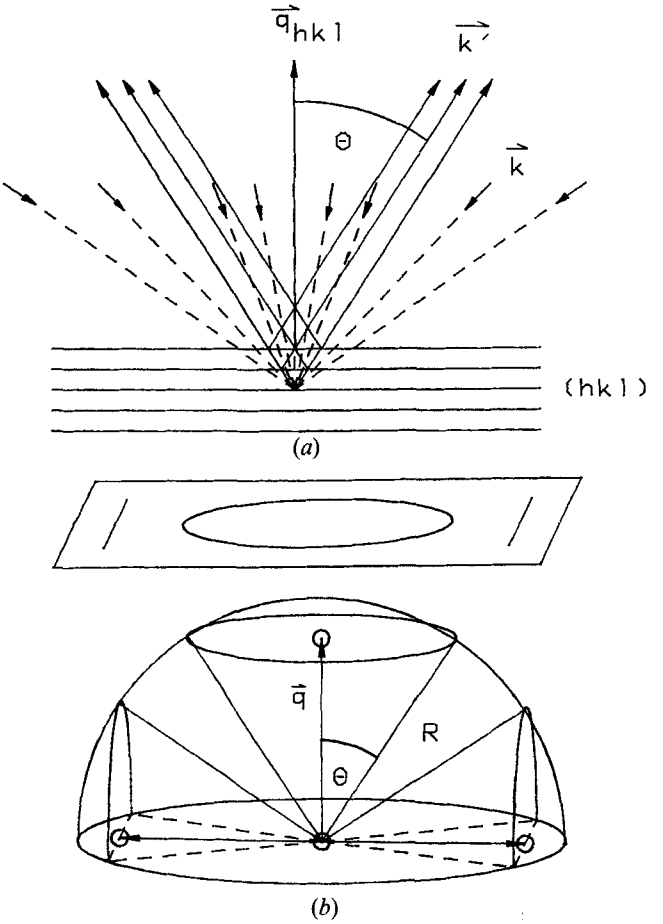

Figure 1. Principle of the Kossel effect. (*a*) A set of planes described by Miller indices (*hkl*) is illuminated with convergent monochromatic light. Scattered beams form a cone (the Kossel cone) determined by the axis perpendicular to the planes and an angle θ which is given by Bragg's law (see equation (1)). (*b*) Construction of the Kossel diagram in reciprocal space (schematically). Each Kossel cone corresponds to a lattice point which is inside the sphere with radius $R = 2|\mathbf{k}| = 4\pi\bar{n}/\lambda$, centred at the origin of the reciprocal lattice. The Kossel diagram is given by the planar projection along the direction of observation for all intersection lines between the sphere and the Kossel cones.

which includes the reciprocal lattice point (h, k, l) and is perpendicular to the corresponding reciprocal lattice vector. Each set of planes therefore creates a circle on the surface of a sphere. The centre of this circle gives the direction of the reciprocal lattice vector and its diameter measures the ratio between the interplanar distance d_{hkl} and the wavelength λ of the monochromatic light. When the wavelength λ is decreased, the diameters of Kossel rings increase and additional rings appear. The spacing d_{hkl} can be easily measured by determining the wavelength corresponding to $\theta = 0$.

The Kossel diagram which can be observed in this experiment (§ 3) is the projection of the Kossel lines from the surface of the sphere to a plane perpendicular to the viewing direction. It consists of circles, ellipses and straight lines corresponding to reciprocal lattice vectors parallel, oblique and perpendicular to this direction, respectively.

3. Experimental

For studies on monocrystals, mixtures exhibiting a large temperature range with a blue phase–isotropic phase coexistence region are useful. These systems can be obtained by mixing a chiral mesogenic compound with a nematic component. Here, mixtures of the chiral compound S-(−)-4-[(-methyl-heptyl)-oxybenzoyl]-4-*n*-hexyloxybenzoate (S 811; Merck, Germany)

(1)

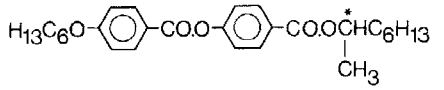

with the nematic mixture EN 18 (Chisso Corporation, Japan) [13] and mixtures of 1,4-bis-[4-(2-methylbutyl)-benzoyloxy]-2-chlorobenzene

(2)

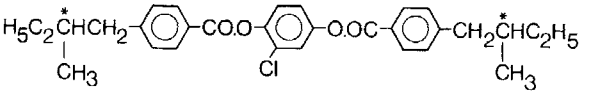

with the nematic mixture ZLI 2585 (Merck) [13] are investigated. For the latter mixture, the clearing temperatures (T_C = 60–65°C) have been found to be lower than the clearing temperatures for the single components (T_C = 88·7°C for compound **2** and T_C = 71·8°C for ZLI 2585).

In order to study the behaviour of monocrystals in an electric field, samples were contained between the flat end of a glass cylinder coated with evaporated aluminium and a cover slide coated with a transparent conducting material. The temperatures of the two surfaces were controlled separately with an accuracy of ±0·01°C by Peltier elements. The sample thickness was adjusted between 10 and 30 μm. Alternating voltages up to 80 V with frequencies between 1 and 5 kHz were applied.

Kossel diagrams were obtained using an inverted metallurgical microscope (type PME, Olympus) equipped with an immersion objective (numerical aperture 1·3). The sample was illuminated through the objective with convergent beams of monochromatic light and the focal plane of the objective was observed by removing the eyepiece or by using a Bertrand lens. Due to reflection at the aluminium surface two superimposed Kossel diagrams were observed, with one being an inversion of the other through the centre of the diagram. Thus, for a crystal oriented with its [211] axis (no rotation axis) parallel to the viewing direction, a Kossel diagram with two-fold symmetry was observed. For a [111] oriented crystal (three-fold axis) the Kossel diagram has six-fold symmetry. Possibilities to distinguish between [111] oriented crystals of BP I or BP II and a hexagonal phase are discussed in § 4.

For measurements of the macroscopic selective reflection, cells with TN-type surface treatment (Videlec) were filled with blue phase material. Voltages up to 40 V at 1 kHz were applied to samples of thickness 9 μm. The temperature was controlled by a Haake F3-S thermostat and measured separately with chromel–alumel thermocouples. Samples were illuminated with white circularly polarized light and the spectra of the backscattered light were detected by means of a PR 702 A multielement spectroradiometer (Photo-Research).

4. Results

The investigation of Kossel diagrams shows that BP I and BP II in the mixtures under investigation exhibit body centred cubic (b.c.c.) and simple cubic (s.c.)

structures, respectively, as found for all other systems investigated so far. Kossel lines corresponding to (110), (200) and (211) planes were observed for BP I, (100) and (110) lines for BP II.

When single crystals are grown in the electric field, the four-fold axis is aligned parallel to the field direction for BP I and BP II. For [100] oriented crystals, the lattice constant in the field direction increases with increasing field strength for BP I and decreases for BP II (as found in [10]), leading to the deformed structures BP I^d and BP II^d which are described by tetragonal space groups. In addition to the findings of [10], a hexagonal phase (BPH) was observed in an electric field. The shape of the monocrystals (see figure 2 (*b*)) and the Kossel diagram (see figure 2 (*d*)) for BPH show a six-fold axis along the field direction. This is the first observation of a field-induced transition between different blue phase modifications for systems with $\varepsilon_a < 0$. BP I^d as well as BP II^d can be transformed to BPH.

In the Kossel diagrams of BPH the following sequence of lines appears with decreasing wavelength:

(*a*) a central ring corresponding to a wavevector along the field direction,
(*b*) six straight lines forming a regular hexagon which correspond to wavevectors perpendicular to the field direction and
(*c*) six ellipses which appear when the central ring intersects the straight lines. (On the photographs in figures 2 (*d*) and 4 (*a*) only half of the Kossel diagram is seen due to the presence of a screen which is used in order to increase the contrast; the complete Kossel diagram exhibits inversion symmetry, as the theoretical diagrams represented in figure 4 (*a*).)

This sequence is expected for the thirteen wavevectors as represented in figure 3 (*b*). The lattice constants c and a, parallel and perpendicular to the field direction, respectively, can be determined from the two wavelengths

$$\lambda_{0001} = 2\bar{n}c \quad \text{and} \quad \lambda_{10\bar{1}1} = \frac{2\bar{n}}{\left(\frac{1}{c^2} + \frac{4}{3}\frac{1}{a^2}\right)^{1/2}}, \tag{3}$$

where the central (0001) ring and the (10$\bar{1}$1) ellipses appear, respectively. Unlike the three dimensional BPH observed in systems with $\varepsilon_a > 0$ [4], the ratio c/a is found to be smaller than unity. For a mixture of 22·1 per cent of compound **1** in EN 18 the typical value of

$$\frac{c}{a} = \frac{3^{1/2}}{2}\left[\left(\frac{\lambda_{0001}}{\lambda_{10\bar{1}1}}\frac{\bar{n}(\lambda_{10\bar{1}1})}{\bar{n}(\lambda_{0001})}\right)^2 - 1\right]^{1/2} \tag{4}$$
$$= 0{\cdot}8$$

is obtained. (The dispersion of the refractive index was measured using a Leitz–Jelley refractometer.) The (0001) reflection band observed for normal incidence is left circularly polarized for mixtures of compound **1** and right circularly polarized for mixtures exhibiting compound **2**.

Although in our experimental set-up Kossel diagrams with six-fold symmetry were obtained for [111] oriented crystals of BP I and BP II due to reflection at the aluminium coated second interface of the sample, BPH can be clearly distinguished from BP I and BP II (see figure 4). The most obvious difference of the Kossel diagrams is the appearance of the central (0001) ring for BPH, while the first central rings

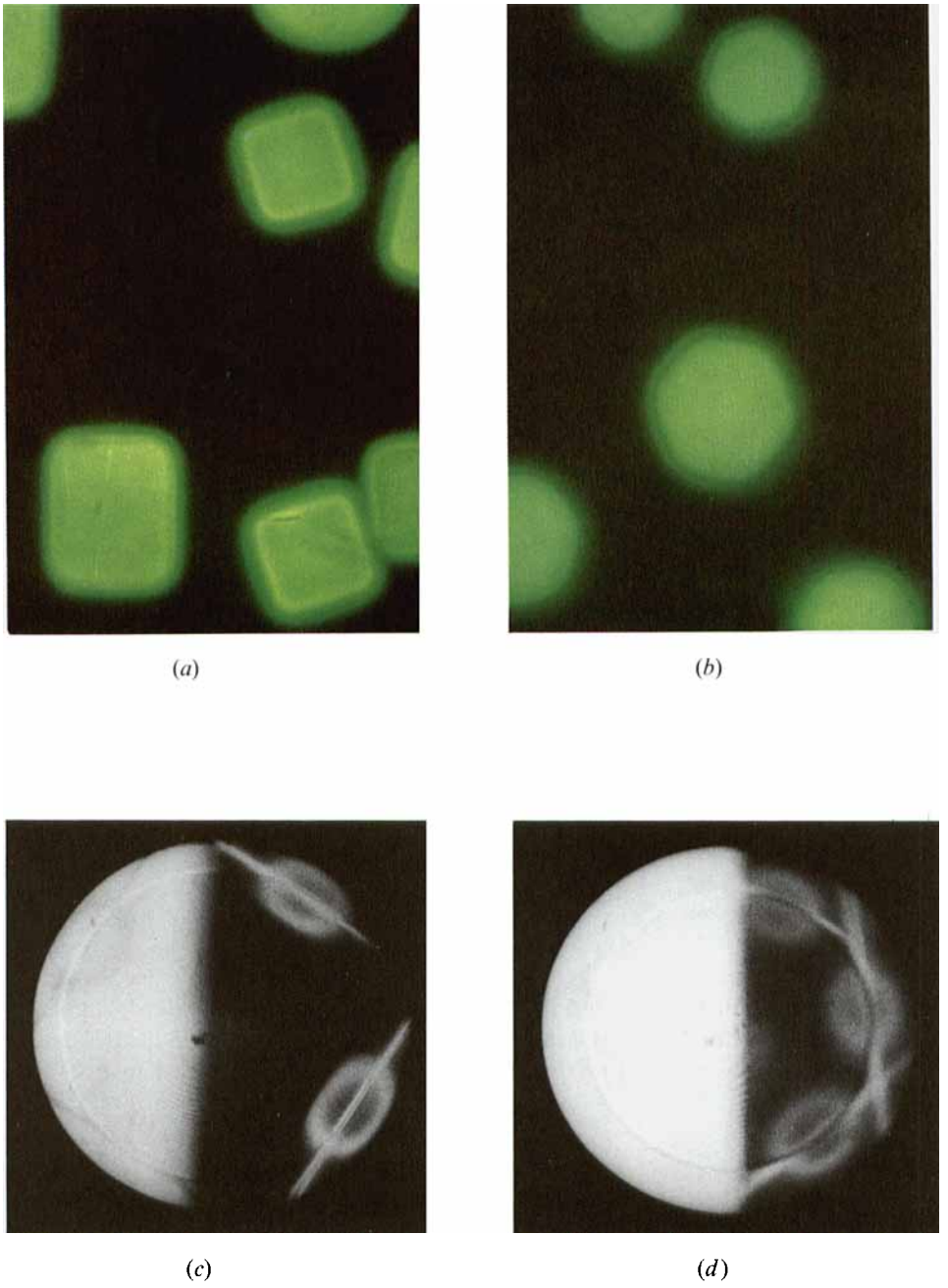

Figure 2. The shape of monocrystals observed in the electric field by polarizing microscopy for a mixture of 25·5 wt % of compound **1** in EN 18: (*a*) BP II^{d} ($E < 2{\cdot}79 \times 10^{6}\,\mathrm{V\,m^{-1}}$); (*b*) the hexagonal phase BPH ($2{\cdot}7\,\mathrm{g} \times 10^{6}\,\mathrm{V\,m^{-1}} < E < 3{\cdot}53 \times 10^{6}\,\mathrm{V\,m^{-1}}$). Respective Kossel diagrams for the same mixture: (*c*) BP II^{d}, $E < 2{\cdot}79 \times 10^{6}\,\mathrm{V\,m^{-1}}$, $\lambda = 428\,\mathrm{nm}$; (*d*) BPH, $E > 2{\cdot}79 \times 10^{6}\,\mathrm{V\,m^{-1}}$, $\lambda = 434\,\mathrm{nm}$. (In order to increase the contrast between the Kossel lines and the background, half of the Kossel diagram was darkened by introducing an opaque screen in the focal plane of the condenser; the complete Kossel diagram exhibits inversion symmetry as the theoretical diagrams represented in figure 4 (*a*).)

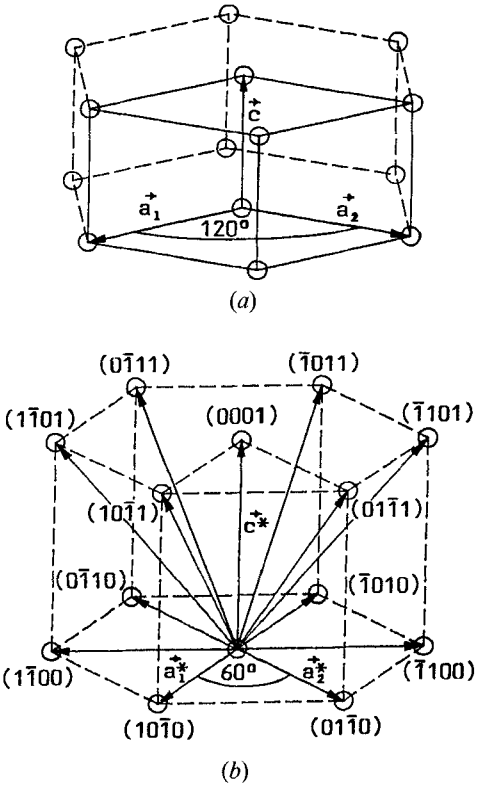

Figure 3. Description of the hexagonal structure. (*a*) Unit cell (solid lines) of the real lattice, characterized by the lattice constants $a = |\mathbf{a}_1| = |\mathbf{a}_2|$ and $c = |\mathbf{c}|$. (*b*) Reciprocal lattice. The lengths of the basis vectors $\mathbf{a}_1^*$, $\mathbf{a}_2^*$, $\mathbf{c}^*$ are related to the lattice constants by $a^* = |\mathbf{a}_1^*| = |\mathbf{a}_2^*| = 4\pi/(3^{1/2}a)$ and $c^* = |\mathbf{c}^*| = 2\pi/c$. The 13 Kossel lines which have been observed experimentally (see figure 2 (*d*)) correspond to the wavevectors $\mathbf{q}_{hkil}$ which are labelled using the Bravais–Miller convention with $i = -(h + k)$.

expected for BP I and BP II appear at wavelengths $\lambda_{222} = 0{\cdot}577\bar{n}a$ and $\lambda_{111} = 1{\cdot}155\bar{n}a$, respectively. For the Kossel diagrams of BP I and BP II oriented with the three-fold axis in the field direction no significant continuous change under the influence of an electric field have been observed. At sufficiently high field strengths [111] oriented monocrystals of BP I and BP II disappear due to the movement of grain boundaries. Only [001] oriented crystals of BP I^d and BP II^d are observed at a field strength slightly lower than the value $E_{\text{BP-BPH}}$ where BPH is induced.

Figure 5 shows the variation of the selective reflection with the electric field for a mixture of compound **1** (22·6 per cent) with EN 18 where the coexistence of BP I and BP II can be observed due to a weak temperature gradient. BP I^d and BP II^d are transformed to BPH at the same field strength $E_{\text{BP I}^d\text{-BPH}} = E_{\text{BP II}^d\text{-BPH}} = E_{\text{BP-BPH}}$. For neither transition was a discontinuity of the wavelength of selective reflection in the field direction observed. This behaviour indicates that at the transition the lattice constant c of BPH is equal to the lattice constant of BP II^d and to half of the lattice constant of BP I^d in the field direction, respectively.

In the Kossel diagrams the (002) ring of BPI^d and the (001) ring of BP II^d become the (0001) ring of BPH without a change of diameter. Moreover, a relation of the orientations of the wavevectors perpendicular to the field direction has been observed

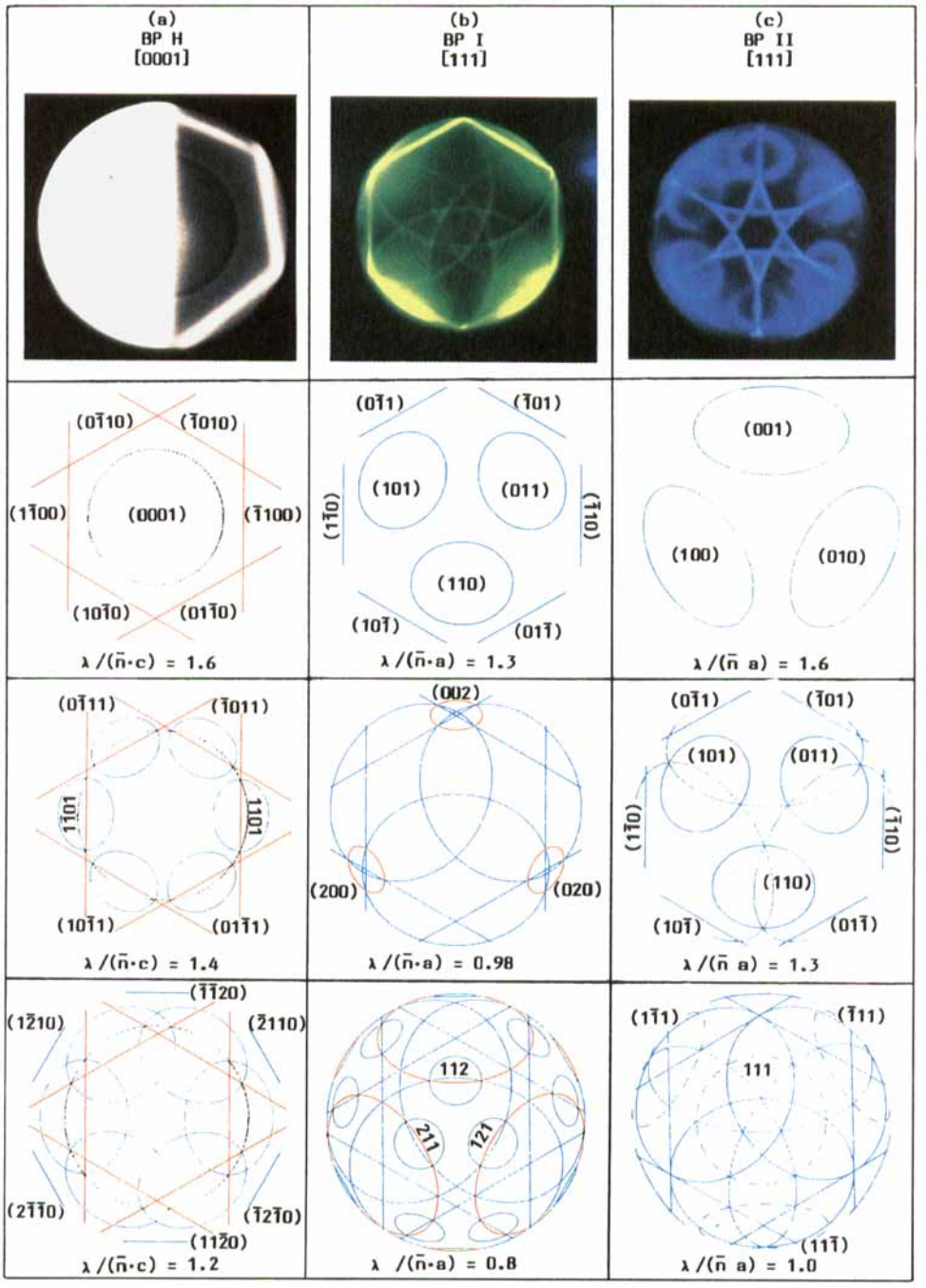

Figure 4.

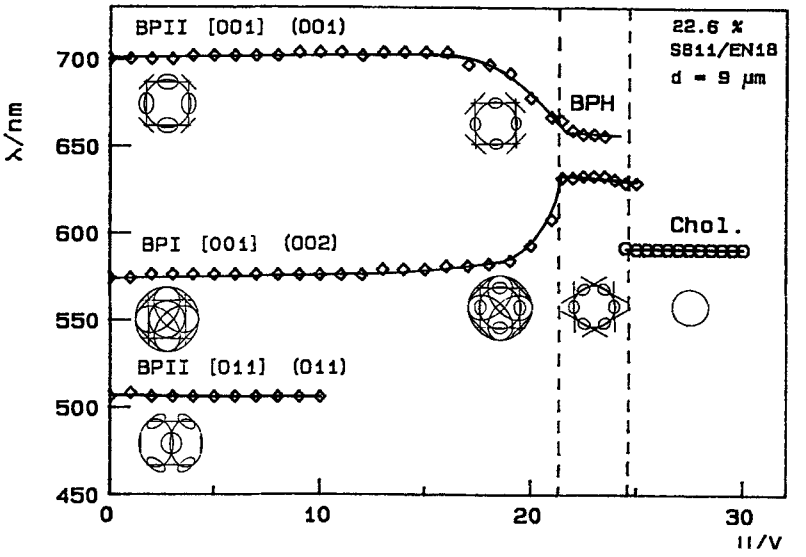

Figure 5. Variation of the wavelength λ_{hkl} of Bragg peaks in the electric field, measured with the spectral scanner in back reflection. Miller indices (*hkl*) describe the corresponding set of planes, indices [*HKL*] indicate the orientation of BP I and BP II crystals with respect to the field direction. The respective Kossel diagrams are calculated for constant wavelength with $\lambda/(\bar{n}a_{\mathrm{BP\,I}}(0\,\mathrm{V})) = 0{\cdot}61\lambda/(\bar{n}a_{\mathrm{BP\,II}}(0\,\mathrm{V})) = 0{\cdot}82$.

for the BP II$^{\mathrm{d}}$–BPH transition (as reported in [7] for systems with $\varepsilon_{\mathrm{a}} > 0$) as well as for the BPI$^{\mathrm{d}}$–BPH transition. In the latter case one opposite pair of wavevectors equivalent to [110] in BP I is transformed to one pair of wavevectors equivalent to [10$\bar{1}$0] in BPH without change of direction.

In figure 5 the different values for the wavelength λ_{0001} of BPH obtained from BP I$^{\mathrm{d}}$ and BP II$^{\mathrm{d}}$ can be explained by the temperature dependence of the lattice constant c of BPH (see figure 6) which is found to increase continuously with increasing temperature. A phase diagram in the E/T plane representing the transition temperatures determined at constant field strength for a mixture of compound **1** and EN 18 is given in figure 7. The threshold field strengths $E_{\mathrm{BP\text{-}BPH}}$ where BPH becomes stable and $E_{\mathrm{BP\text{-}Ch}}$ where the cholesteric phase is induced, increase with increasing chirality (see table 1). In the system compound **2**–ZLI 2585, BPH is observed only for mixtures with relatively high concentrations ($\geqslant 40$ per cent) of the chiral compound, whereas in the system compound **1**–EN 18 the BP I$^{\mathrm{d}}$–BPH transition also occurs for mixtures with low chiral concentration which exhibit no BP II.

Figure 4. Experimental Kossel diagrams with six-fold symmetry and comparison with theory. (*a*) BPH (25·5 wt % of compound **1** in EN 18, $E = 33{\cdot}2\,\mathrm{V}(11\,\mu\mathrm{m})^{-1}$, $\lambda = 462\,\mathrm{nm}$); (*b*) BP I, [111] axis ∥ surface normal (23·5 wt % compound **1**, $E = 0$, $\lambda = 568\,\mathrm{nm}$); (*c*) BP II, [111] axis ∥ surface normal 23·5 wt % of compound **1**, $E = 0$, $\lambda = 483\,\mathrm{nm}$). Although [111] is a three-fold axis for BP I and BP II, six-fold symmetry is observed experimentally due to reflection at the electrode surface. However, the Kossel diagrams differ considerably compared with BPH. For the photograph of BPH, half of the Kossel diagram was darkened by a screen in order to increase the contrast; by rotating the screen inversion symmetry of the Kossel diagram was observed, in agreement with the theoretical diagrams. The theoretical diagrams for BPH are calculated using $c/a = 0{\cdot}8$ for the ratio of the lattice constants parallel and perpendicular to the field direction.

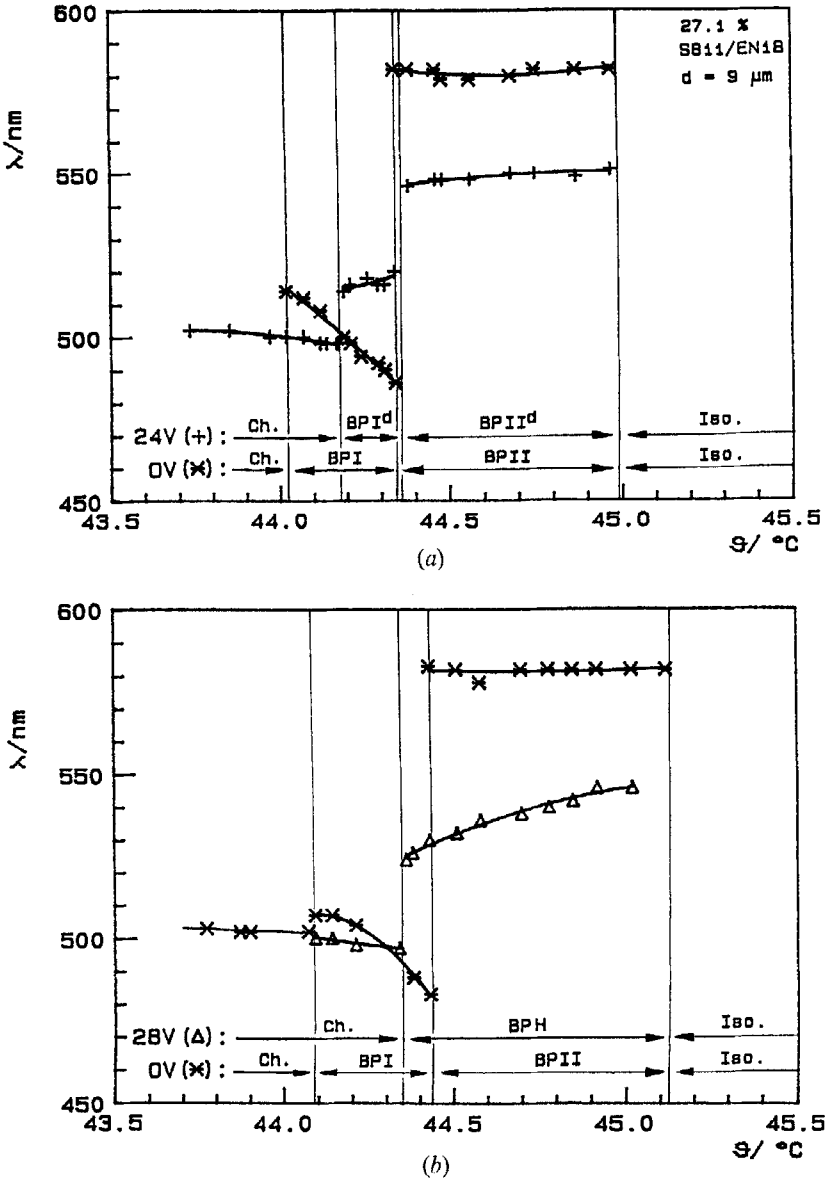

Figure 6. Wavelength $\lambda_{hkl}(E)$ of Bragg peaks measured in back reflection for increasing temperature at constant field strength E for values (*a*) lower and (*b*) higher then the threshold $E_{BP\text{-}BPH}$. For comparison with the transition temperatures observed in the absence of the field, the diagrams contain the values $\lambda_{hkl}(0)$ which are measured simultaneously at a spot outside the conductive coated area of the sample surface (*).

Because of large time constants for the reorientation of monocrystals anchored at the surface of the sample, it was also possible to investigate the deformation of BP I and BP II for orientations other than [001] ‖ **E**. Investigations on the interplanar spacing of the (001) planes in BP II for different orientations show that the relative change $\delta \equiv |(d_{001}(E) - d_{001}(0)|/d_{001}(0)$ at constant field strength E decreases with increasing angle ϕ between the [001] axis and the field direction. $\delta = 0$ is observed for [111] ‖ **E** ($\phi = 54{\cdot}7°$). Additionally, the (110) interplanar spacing in BP II for the

Table 1. Composition of the mixtures investigated, threshold field strength (r.m.s.) for the field-induced transitions from the deformed cubic BP I^{d} or BP II^{d} to the hexagonal structure BPH, and field strength for the phase transition from the blue phase occurring at high field strength close to the clearing temperature (BP I^{d} or BP II^{d} or BPH) to the cholesteric phase.

Chiral compound	Nematic component	Concentration of the chiral component (per cent by weight)	Blue phases occurring in the mixture for $E = 0$ V	$E_{\text{BP Id-BPH}}$ or $E_{\text{BP IId-BPH}}/10^{6}\,\text{V m}^{-1}$	$E_{\text{BP-Ch}}/(10^{6}\,\text{V m}^{-1})$	Frequency/kHz of the applied voltage
1	EN 18	22·1	BP I	1·73	1·88	1
1	EN 18	22·6	BP I, BP II	2·34	2·72	1
1	EN 18	25·5	BP I, BP II	2·79	3·53	1
1	EN 18	27·1	BP I, BP II	2·84	3·95	1
2	ZLI 2585	33·7	BP I	–	2·00	5
2	ZLI 2585	37·0	BP I, BP II	–	2·91	5
2	ZLI 2585	40·0	BP I, BP II	~3·2	3·28	5
2	ZLI 2585	43·0	BP I, BP II	3·80	4·07	5

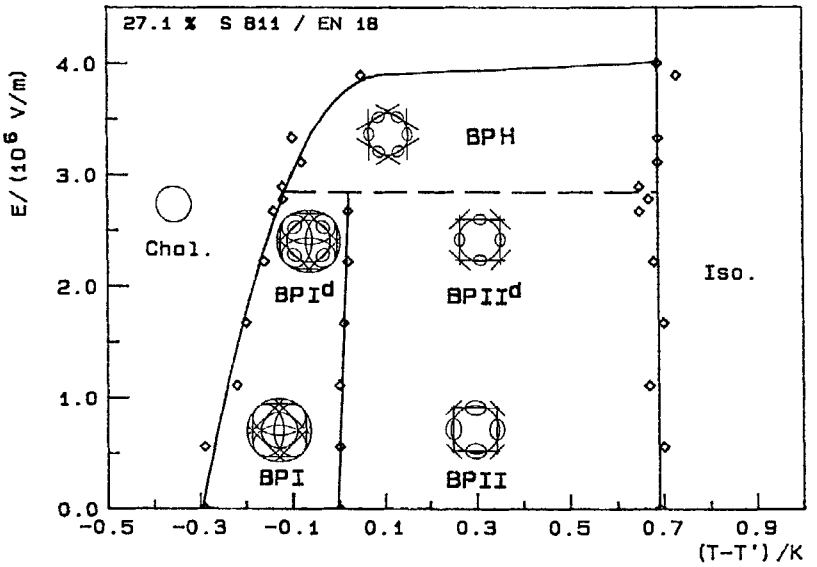

Figure 7. Phase diagram in the E/T plane, obtained by observation of selective reflection with increasing temperature at constant field strength. In order to obtain reproducible values, two spots inside and outside of the electrode area of the sample have been observed simultaneously and differences $(T - T')$ are measured, where T' is the temperature of the BP I–BP II transition at $E = 0$. The Kossel diagrams appearing for the respective coordinates in the phase diagram are given for constant wavelength λ with the same parameter as used in figure 5.

Table 2. Shift of the wavelength λ_{hkl} of selective reflection observed in the electric field for BP I and BP II due to continuous deformation of the cubic structure.

Phase (space group)	Orientation of the unit cell, $[hkl] \parallel \mathbf{E}$	Effect observed for materials with $\varepsilon_a > 0$		Effect observed for materials with $\varepsilon_a < 0$		Space group of the deformed structure
BP I ($I4_132/O^8$)	[100]	$\frac{d\lambda_{200}}{dE} < 0$	[15]	$\frac{d\lambda_{200}}{dE} > 0$	[10]	$I4_122/D_4^{10}$
BP I ($I4_132/O^8$)	[110]	$\frac{d\lambda_{110}}{dE} > 0$	[2]	$\frac{d\lambda_{110}}{dE} < 0$	[10]	$F222/D_2^7$
BP II ($P4_232/O^2$)	[100]	$\frac{d\lambda_{100}}{dE} > 0$	[2]	$\frac{d\lambda_{100}}{dE} < 0$	[10]	$P4_222/D_4^5$
BP II ($P4_232/O^2$)	[110]	$\frac{d\lambda_{110}}{dE} > 0$	[3]	$\frac{d\lambda_{110}}{dE} < 0$	(see figure 8)	$C222/D_2^6$

Figure 8. Kossel diagrams for BP II oriented with the [110] axis along the viewing direction (mixture of 23·5 wt % of compound **1** in EN 18, $\lambda = 501$ nm, $d = 10\,\mu$m): (*a*) $U = 0$ V, (*b*) $U = 17{\cdot}7$ V. A decrease of the periodicity in the [110] direction with increasing field strength is indicated by the shrinking of the (110) ring in the centre of the diagram.

(*a*)

(*b*)

Figure 8.

orientation [110] ‖ **E** has been found to decrease with increasing field strength (see figure 8). For comparison with previous studies, the effects observed for BP I and BP II, depending on the sign of ε_a, are summarized in table 2.

5. Discussion and conclusion

5.1. *Structure of the hexagonal phase, phase transitions BP I^d–BPH and BP II^d–BPH*

The observation of (0001) and (10$\bar{1}$1) lines in the Kossel diagrams show that BPH observed in the systems under investigation has to be described by a three dimensional chiral hexagonal space group. According to the selection rules gives in table 1 of [7], only $P6_2$ ($P6_4$) and $P6_222$ ($P6_422$) have to be taken into account as the (0001) reflection band is circularly polarized and can be observed for normal incidence. For $\varepsilon_a > 0$ it has been shown [7] that shearing of the unit cell of BP II^d leads by a continuous transition to the space group $P6_222$. These symmetry arguments are also valid for systems with $\varepsilon_a < 0$, although the lattice constant in the field direction is shortened for these materials. It can be concluded that the hexagonal structures BPH^{3D} observed here are described by the space groups $P6_222$ (D_6^4) and $P6_422$ (D_6^5) (depending on the sign of the chirality), respectively, and that the continuous transition BP II^d–BPH^{3D} can be described by a shearing of the unit cell as proposed for systems with $\varepsilon_a > 0$ [7].

However, for the transition BP I^d–BPH^{3D} no continuous variation from the tetragonal space group $I4_122$ (D_4^{10}) to the hexagonal space group $P6_222$ (D_6^4) can be considered without appearance of additional nodes in the unit cell at the transition. Since the periodicities d_{002} and d_{110} of the cubic lattice become the interplanar distances d_{0001} and $d_{10\bar{1}0}$ of the hexagonal lattice, the ratio of the unit cell volumes, $V_{BPH}/V_{BP\,I}$, is approximately 1/4.

Recently, the stability of three dimensional BPH structures in an electric field has been considered theoretically for materials with $\varepsilon_a > 0$ [9]. Two different structures H_a^{3D} and H_b^{3D} of the space group $P6_222$ are proposed to appear in the field whereas a $P6_122$ structure is not stabilized by the field. The wavevectors $\mathbf{q}_{\sigma_h}$, $\mathbf{q}_{\sigma_b}$ and $\mathbf{q}_{\sigma_d}$ used in the model of Hornreich and Shtrikman [9] are equivalent to (0001), (10$\bar{1}$0) and (10$\bar{1}$1) observed experimentally (see figures 2 (*d*) and 4 (*a*)). Since the structures H_a^{3D} and H_b^{3D} differ only in their phase factors, they cannot be distinguished in our experiment. Neither the occurrence of BPH^{3D} for systems with $\varepsilon_a < 0$ nor a transition BP I–BPH^{3D} has been considered theoretically, so far.

5.2. *Deformation of BP I and BP II for a 'weak' electric field*

Recently Porsch and Stegemeyer [16] have shown that the deformation of BP I in the electric field can be described with satisfactory accuracy if the strain tensor ε_{ij} is assumed to be quadratic in E:

$$\varepsilon_{ij} = \sum_{k=1}^{3} \sum_{l=1}^{3} \gamma_{ijkl} E_k E_l \tag{5}$$

In this case, the distortion is completely described by the fourth rank electrostriction tensor γ_{ijkl} which, for cubic symmetry, exhibits three independent coefficients [17]. Using this approximation the behaviour of the (100) peak for BP II crystals of different orientation observed in our experiment can be shown to be equivalent to a constant volume of the unit cell during the deformation, i.e.

$$\varepsilon_{11} + \varepsilon_{22} + \varepsilon_{33} = 0 \tag{6}$$

and the relation

$$\gamma_{1122} = -\tfrac{1}{2}\gamma_{1111} \tag{7}$$

can be concluded. Thus, only two independent coefficients of the electrostriction tensor remain which can be calculated from the numerical values for the effects represented in table 2. A detailed presentation will be given in a forthcoming paper [18].

5.3. *Orientation of blue phases in the electric field*

As we have mentioned, BP I and BP II in the mixtures under investigation are preferentially oriented with one of the four-fold axes parallel to the field direction. The same behaviour was observed for systems with $\varepsilon_a > 0$ except for BP I in mixtures showing the field-induced transition from BP I to the tetragonal structure BPX [1]. In a previous paper [19] the orientation of blue phases has been discussed by considering the torque $\mathbf{\Gamma}$ acting on monocrystals due to the anisotropic part of the fourth rank susceptibility tensor χ_{ijkl}. It has been shown that $\mathbf{\Gamma}$ can be written as

$$\mathbf{\Gamma} = VA \sum_{i=1}^{3} (\mathbf{n}_i \cdot \mathbf{E})^3 (\mathbf{n}_i \times \mathbf{E}), \tag{VIII}$$

where $\mathbf{n}_1$, $\mathbf{n}_2$ and $\mathbf{n}_3$ are unit vectors parallel to the four-fold axes of the crystal, V is the volume of the crystal and A is a parameter characterizing the material. The torque vanishes if the [100], [110] or [111] direction is parallel to $\mathbf{E}$ and the absolute stable orientation can be either [100] $\parallel \mathbf{E}$ or [111] $\parallel \mathbf{E}$, depending on the sign of the parameter A. However, no theoretical attempt has been made so far to calculate this parameter from the properties of the material, such as the dielectric anisotropy and the elastic coefficients. The results presented here show that A is positive for BP I and BP II occurring in systems with $\varepsilon_a < 0$ as observed for the mixtures with $\varepsilon_a > 0$ investigated in [19].

We thank Michaela Wolff for preparation of the chiral compound **2** and E. Merck for supplying us with ZLI 2585. G. Heppke and H. Kitzerow thank the Laboratoire de Physique des Solides, Orsay, for their kind hospitability. The authors thank Professor Peter Crooker for critical reading of the manuscript. Financial support by the Deutsche Forschungsgemeinschaft (Sonderforschungsbereich 335, 'Anisotrope Fluide') is gratefully acknowledged.

References

[1] For a review, see: STEGEMEYER, H., BLÜMEL, TH., HILTROP, K., ONUSSEIT, H., and PORSCH, F., 1986, *Liq. Crystals*, **1**, 3. For comments: PIERANSKI, P., and CLADIS, P. E., 1988, *Liq. Crystals*, **3**, 397. STEGEMEYER, H., BLÜMEL, TH., and ONUSSEIT, H., 1988, *Liq. Crystals*, **3**, 399.

[2] HEPPKE, G., KRUMREY, M., and OESTREICHER, F., 1983, *Molec. Cryst. liq. Cryst.*, **99**, 99.

[3] HEPPKE, G., KITZEROW, H.-S., and KRUMREY, M., 1987, *Molec. Crystals liq. Crystals*, **150b**, 265.

[4] PIERANSKI, P., and CLADIS, P. E., 1987, *Phys. Rev.* A, **35**, 355.

[5] PIERANSKI, P., CLADIS, P. E., and BARBET-MASSIN, R., 1985, *J. Phys., Paris, Lett.*, **46**, L-973.

[6] JORAND, M., and PIERANSKI, P., 1987, *J. Phys., Paris*, **48**, 1197.

[7] JÉRÔME, B., and PIERANSKI, P., 1989, *Liq. Crystals*, **5**, 799.

[8] HORNREICH, R. M., KUGLER, M., and SHTRIKMAN, S., 1985, *Phys. Rev. Lett.*, **54**, 2099.

[9] HORNREICH, R. M., and SHTRIKMAN, S., 1989, *Liq. Crystals*, **5**, 777.
[10] HEPPKE, G., KITZEROW, H.-S., and KRUMREY, M., 1985, *Molec. Crystals liq. Crystals Lett.*, **1**, 117.
[11] HEPPKE, G., KITZEROW, H.-S., and KRUMREY, M., 1985, *Molec. Crystals liq. Crystals Lett.*, **2**, 59.
[12] KOSSEL, W., LOECK, V., and VOGES, H., 1935, *Z. Phys.*, **94**, 139.
[13] EN 18 (Chisso Corporation) is a commercially available nematic mixture exhibiting a dielectric anisotropy of $\varepsilon_a \approx -6$ for $T = 298\,K, f = 1\,kHz$. ZLI 2585 (Merck) consists of bicyclohexylcarbonitriles with the cyano group in the axial position ($\varepsilon_a \approx -8$ for $T = 298\,K, f = 5\,kHz$).
[14] LUBIN, D., and HORNREICH, R. M., 1987, *Phys. Rev.* A, **36**, 849.
[15] HEPPKE, G., JÉRÔME, B., KITZEROW, H.-S., and PIERANSKI, P., 1989, *Europhysics Lett.* (submitted).
[16] PORSCH, F., and STEGEMEYER, H., 1988, Elektrostriktion der Blauen Phasen', Bericht zum Doktorandenkolloquium 'Anisotrope Fluide', p. 104, Technische Universität Berlin.
[17] NYE, J. F., 1957, *Physical Properties of Crystals* (Clarendon Press).
[18] HEPPKE, G., JÉRÔME, B., KITZEROW, H.-S., and PIERANSKI, P., 1989, *J. Phys. Paris*, **50**(3) (in the press).
[19] PIERANSKI, P., CLADIS, P. E., GAREL, T., and BARBET-MASSIN, R., 1986, *J. Phys., Paris*, **47**, 139.